

# 中国激光

## 结构紧凑的高均匀性硅波导阵列波导光栅

封治华<sup>1,4</sup>, 袁硕<sup>2</sup>, 陈益姝<sup>2</sup>, 刘海鹏<sup>2</sup>, 毕群玉<sup>3</sup>, 张福领<sup>4\*</sup>, 冯吉军<sup>2\*\*</sup>

<sup>1</sup> 西安电子科技大学物理学院, 陕西 西安 710071;

<sup>2</sup> 上海理工大学上海市现代光学系统重点实验室, 上海 200093;

<sup>3</sup> 苏州大学江苏省先进光学制造技术重点实验室, 江苏 苏州 215006;

<sup>4</sup> 中国电子科技集团公司第二十七研究所, 河南 郑州 450047

**摘要** 基于绝缘体上硅材料平台, 设计并制作了一种结构紧凑的高均匀性硅波导阵列波导光栅, 其拥有 8 个输出通道并且通道间隔为 200 GHz。分析了绝缘体上硅材料平台中硅波导的弯曲半径对弯曲损耗和有效折射率的影响。测试结果表明, 该器件的插入损耗为 19.6 dB, 串扰为 -15 dB, 非均匀性为 0.87 dB, 3 dB 带宽为 1.06 nm, 结构尺寸仅为 294 μm × 190 μm。芯片的制作工艺与互补金属氧化物半导体工艺兼容, 这使得阵列波导光栅的大批量、低成本生产成为可能, 对集成波分复用网络的发展具有重要的意义。

**关键词** 集成光学; 阵列波导光栅; 结构紧凑; 硅基波导; 波分复用

中图分类号 O436

文献标志码 A

DOI: 10.3788/CJL230484

### 1 引言

随着大流量网络的快速发展, 人们对数据交换速率的需求日益提升<sup>[1]</sup>。在光通信网络中, 波分复用(WDM)因通信速度快、传播信号透明、有效拓展了传播容量并且成本低等特点而备受关注<sup>[2-3]</sup>。密集波分复用(DWDM)进一步拓展了通信系统的通信容量, 满足了人们对日益增长的通信带宽的需求, 成为了光通信领域的重要组成部分<sup>[4-6]</sup>。阵列波导光栅(AWG)具有串扰低、插入损耗低、均匀性高、可靠性高、结构紧凑等优点, 成为密集波分复用最常用的技术方案<sup>[7-12]</sup>。

阵列波导光栅自 1988 年被 Smit<sup>[13]</sup> 提出以来, 得到了广泛的研究, 并且在许多材料中被验证, 如 InP<sup>[14]</sup>、SiO<sub>2</sub><sup>[15]</sup> 和聚合物<sup>[16]</sup> 等。Li 等<sup>[17]</sup> 采用 SiO<sub>2</sub> 材料, 制作了含有 8 个输出通道并且通道间隔为 800 GHz 的阵列波导光栅, 其尺寸为 11 mm × 4 mm。Min 等<sup>[18]</sup> 采用聚合物材料平台制作了含有 16 个输出通道并且通道间隔为 100 GHz 的阵列波导光栅, 其尺寸为 22 mm × 27 mm。这些材料的芯层和包层的折射率对比度较低, 因此器件的尺寸和弯曲损耗较大, 这对高度集成的密集波分复用系统的发展是非常不利的<sup>[19-20]</sup>。为了减小器件尺寸和弯曲损耗, 寻找高折射率对比度的阵列波导光栅制作平台是非常有必要的<sup>[21-23]</sup>。硅波导阵列波导光栅

由于具有高的折射率对比度, 其结构能够设计得十分紧凑, 并且其与互补金属氧化物半导体(CMOS)工艺相兼容, 使得阵列波导光栅的大批量、低成本生产成为可能<sup>[24-26]</sup>。目前已经有多采用硅波导的阵列波导光栅被制作出来。Pathak 等<sup>[27]</sup> 采用硅波导制作了含有 12 个输出通道并且通道间隔为 400 GHz 的阵列波导光栅, 其尺寸为 560 μm × 350 μm, 非均匀性为 1.55 dB。Li 等<sup>[28]</sup> 采用硅波导制作了含有 16 个输出通道并且通道间隔为 200 GHz 的阵列波导光栅, 其尺寸为 400 μm × 430 μm, 非均匀性为 4.3 dB。对于目前已有的采用硅波导的阵列波导光栅, 需要完善的地方是进一步减小尺寸以增加集成度, 并改善各输出通道的均匀性。

本文提出了一种结构紧凑的高均匀性硅波导阵列波导光栅, 分析了硅波导的弯曲半径对弯曲损耗和有效折射率的影响, 设计并制备了含有 8 个输出通道并且通道间隔为 200 GHz 的阵列波导光栅芯片。测试结果表明, 该器件的插入损耗为 19.6 dB, 串扰为 -15 dB, 非均匀性为 0.87 dB, 3 dB 带宽为 1.06 nm, 结构尺寸仅为 294 μm × 190 μm。该器件采用与互补金属氧化物半导体工艺相兼容的绝缘体上硅(SOI)技术, 因此其大批量、低成本生产能够实现, 这对集成波分复用网络商业化的发展具有推进作用。

收稿日期: 2023-02-02; 修回日期: 2023-02-23; 录用日期: 2023-03-15; 网络首发日期: 2023-03-25

基金项目: 国家重点研发计划(2022YFE0107400)、国家自然科学基金(11774235, 61705130, 11933005)、上海市科学技术委员会(23010503600)、上海市高校特聘教授(东方学者)岗位计划(GZ2020015)、江苏省先进光学制造技术重点实验室资助项目(KJS2139)

通信作者: \*lidarzhang666@163.com; \*\*fjijun@usst.edu.cn

## 2 结构紧凑的高均匀性硅波导阵列波导光栅的设计、仿真与制备

### 2.1 器件设计与仿真

阵列波导光栅主要由输入/输出波导、输入/输出星形耦合器、阵列波导构成,如图 1(a)所示。光束由输入波导传输到长度为 86 μm 的输入星形耦合器中,并且在输入星形耦合器中发散,发散的光束被阵列波导中的每个波导接收。阵列波导中相邻波导之间存在

相同的长度差 14.25 μm,其作用类似透射式衍射光栅。不同波长的光束通过阵列波导后会在输出星形耦合器像平面上不同位置处聚焦,因此在聚焦处放置输出波导即可实现波长的空间分离。输入/输出星形耦合器一般采用罗兰圆的结构,其结构如图 1(b)所示,输入/输出圆的半径是阵列波导孔径的 1/2,并且输入/输出圆的圆心在阵列波导孔径圆上。罗兰圆起到类似凹面光栅聚焦的作用,能消除所有波长下的二阶像差和三阶慧差并且减少衍射畸变<sup>[29]</sup>。

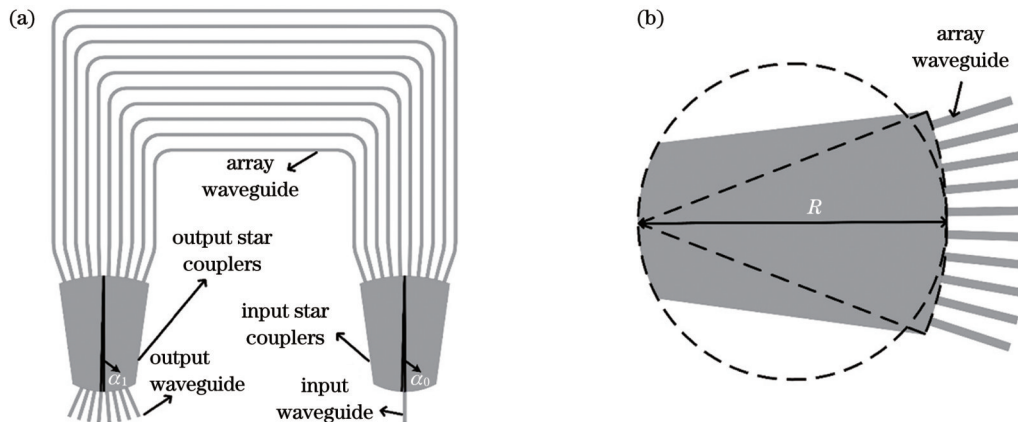


图 1 阵列波导光栅和星形耦合器的示意图。(a)阵列波导光栅结构;(b)星形耦合器结构

Fig. 1 Schematics of arrayed waveguide grating and star coupler. (a) Structure of arrayed waveguide grating; (b) structure of star coupler

阵列波导光栅的基本原理为:由于阵列波导中相邻波导之间存在恒定的长度差,并且该长度差等于中心波长的整数倍,每个阵列波导中波长相同的光束将以相同相位差到达输出星形耦合器,并且输入星形耦合器的光场分布将在输出星形耦合器的像平面上重现。同时,输入星形耦合器中的发散光束在输出星形耦合器像面上会聚,并且会聚后的光束和发散的光束具有相同的振幅和相位分布。由于波导色散的影响,会聚光束的焦点会随着波长的变化而沿输出星形耦合器的像平面移动,因此只需将输出波导放置在输出星形耦合器像面上的适当位置,就可以实现不同波长的空间分离<sup>[30]</sup>。其光栅基本方程为

$$n_s d_a \sin \alpha_0 + n_a \Delta L + n_s d_a \sin \alpha_1 = m\lambda, \quad (1)$$

式中: $n_s$ 、 $n_a$ 分别为星形耦合器、阵列波导的有效折射率; $d_a$ 为阵列波导在星形耦合器切线上的间距; $\alpha_0$ 、 $\alpha_1$ 分别为输入、输出波导相对于阵列波导中心的角度; $m$ 为光栅衍射级次; $\lambda$ 为器件的工作波长<sup>[31]</sup>。阵列波导的色散系数( $D$ )可以表示为

$$D = \frac{dx}{d\lambda} = R \times \frac{N_{gs} d_a \sin \alpha_0 + N_{ga} \Delta L}{n_s d_a \lambda_0}, \quad (2)$$

$$N_{gs} = n_s - \lambda \times \frac{dn_s}{d\lambda}, \quad (3)$$

$$N_{ga} = n_a - \lambda \times \frac{dn_a}{d\lambda}, \quad (4)$$

式中: $x$ 为输出星形耦合器像平面的位置; $R$ 为星形耦合器的长度; $\lambda_0$ 为阵列波导的中心波长; $N_{gs}$ 和 $N_{ga}$ 分别

为星形耦合器和阵列波导的群折射率<sup>[32]</sup>。

在满足式(1)的情况下,随着  $m$  取值的不断变化,  $\lambda$  的取值也会不断变化。因此在相同的入射条件下,同一个端口由于衍射级次的变化而输出不同波长的光,两个波长之差被定义为自由频谱范围,即

$$R_{FSR} = \frac{\lambda^2}{N_{gs} d_a \sin \alpha_0 + N_{ga} \Delta L}. \quad (5)$$

为了使输入星形耦合器中的发散光束在输出星形耦合器像面上会聚,阵列波导中相邻波导之间的长度差  $\Delta L$  应与器件的中心波长的整数倍相等<sup>[33]</sup>, 表示为

$$\Delta L = m \times \frac{\lambda_0}{N_{ga}}. \quad (6)$$

结构紧凑的高均匀性硅波导阵列波导光栅是基于绝缘体上硅的平台,其芯层波导和包层分别是厚度为 220 nm 的硅和厚度为 3 μm 的二氧化硅,两者的折射率分别为 3.476 和 1.444,如图 2(a)所示。为了实现横电(TE)单模传输,波导宽度被设计为 500 nm,这使得波导的传输损耗和器件的整体尺寸较小。图 2(b)所示为 TE 单模波导的模场分布图。阵列波导光栅需要大量的弯曲波导,为了实现更小的弯曲损耗,通常会采用较大的弯曲半径,但这会急剧增加器件的尺寸。对于绝缘体上硅平台的波导结构,其芯层与包层的折射率相差较大,因此波导结构的尺寸和弯曲半径较小。图 3 仿真了硅波导的弯曲半径对弯曲损耗和波导有效折射率的影响。通过仿真结果可知,随着弯曲半径的减小,弯曲损耗和有效折射率先逐渐减小然后稳

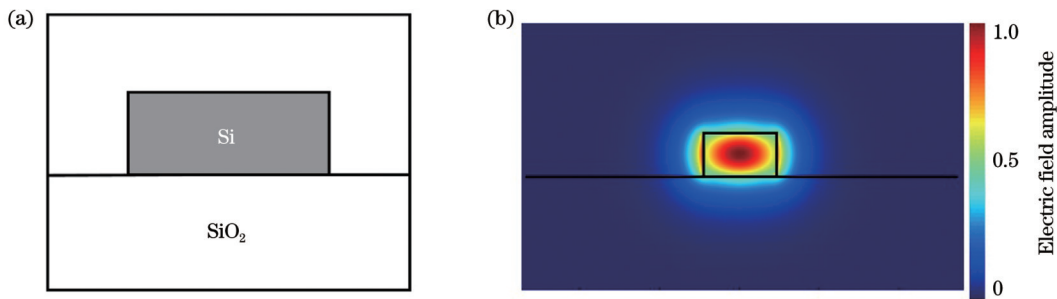


图 2 波导平台和 TE 基模模式。(a) 绝缘体上硅平台;(b)TE 基模场分布

Fig. 2 Waveguide platform and TE fundamental mode. (a) SOI platform; (b) TE fundamental mode field distribution

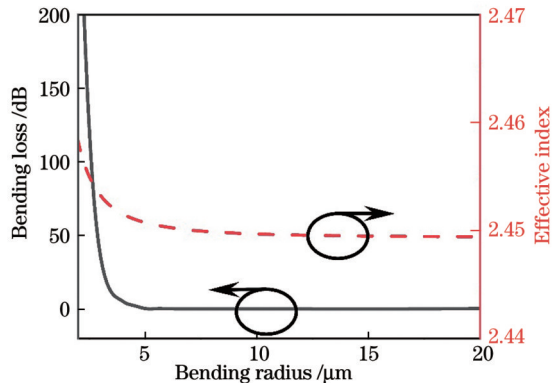


图 3 弯曲损耗和有效折射率随弯曲半径的变化

Fig. 3 Bending loss and effective index versus bending radius

定不变。当弯曲半径为 2.5~5.0  $\mu\text{m}$  时,弯曲损耗大于 1.29 dB,并且硅波导的有效折射率受弯曲半径的影响较大;而当弯曲半径大于 15  $\mu\text{m}$  时,弯曲损耗小于 0.028 dB,基本可以忽略,并且波导的有效折射率稳定在 2.449。根据器件性能综合考量,选取弯曲半径为 15  $\mu\text{m}$ 。根据阵列波导光栅的基本原理和硅波导相关参数,该紧凑高均匀性硅波导阵列波导光栅的主要结构参数如表 1 所示。

表 1 结构紧凑的高均匀性硅波导阵列波导光栅的主要参数

Table 1 Main parameters of compact high uniformity silicon waveguide arrayed waveguide grating

Parameter	Value
Number of channels	8
Center wavelength / nm	1577.5
Channel spacing / nm	1.6
Free spectral range / nm	29.44
Number of arrayed waveguides	43
Minimum bending radius / $\mu\text{m}$	15
Single mode waveguide width / nm	500
Diffraction order	21
Length increment / $\mu\text{m}$	14.05
Pitch of adjacent arrayed waveguides / $\mu\text{m}$	1.2
Length of star coupler / $\mu\text{m}$	86

## 2.2 器件制备

阵列波导光栅芯片制备的具体流程如图 4 所示。首先使用等离子体增强化学气相沉积(PECVD)法在 220 nm 厚的绝缘体上硅晶圆上制备一层二氧化硅(厚度约为 100 nm)。然后在该硅晶圆表面均匀涂抹一层光刻胶(PR)作为掩模材料,接着使用电子束光刻(EBL)法对涂有光刻胶的硅晶圆进行曝光。为了在硅晶圆上显示出器件的结构,需要将曝光后的硅晶圆放入特定的显影液中。在完成显影后利用反应离子刻蚀(RIE)法刻蚀未被光刻胶覆盖的二氧化硅,将电子束光刻胶上的图形转移到二氧化硅上。再用二氧化硅作掩模,利用 RIE 法将二氧化硅中的图形转移到硅波导中。由于波导结构表面还剩余一层薄的二氧化硅,因此还需使用缓冲氢氟酸刻液(BHF)将其去除。在除去表面二氧化硅后,硅基阵列波导光栅的轮廓裸露出来,再利用 RCA 湿法化学清洗方式去除硅波导表面的杂质,最后利用 PECVD 法在硅晶圆表面镀一层二氧化硅包覆层,硅阵列波导光栅芯片制作完成<sup>[34]</sup>。图 5 显示了该阵列波导光栅整体的光学显微镜图,其中图 5(b)~(d) 分别为输入星形耦合器、阵列波导、输出星形耦合器的细节图,白色竖线是其他功能结构的金属电极。

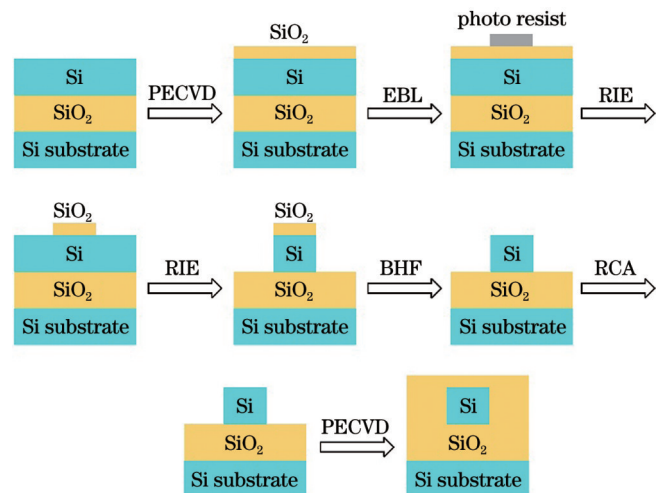


图 4 硅波导阵列波导光栅的制造工艺示意图  
Fig. 4 Schematic of manufacturing process of silicon waveguide arrayed waveguide gratings

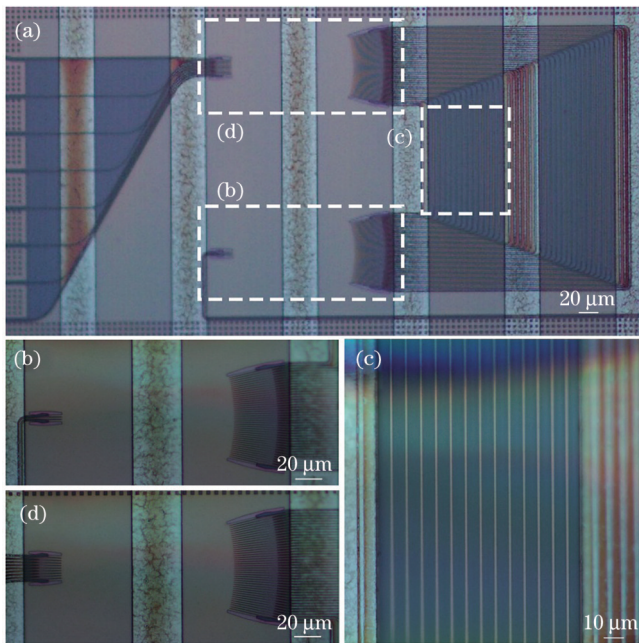


图 5 阵列波导光栅的光学显微镜图

Fig. 5 Optical microscope image of arrayed waveguide grating

### 3 实验分析与讨论

在器件制作完成之后, 对其工作性能进行测试和

表征。图 6 为测试系统的示意图。可调范围为 1565~1625 nm 的激光器发出输入光束, 光束通过光纤传输到偏振控制器。由于阵列波导芯片的设计采用了 TE 基模, 芯片对偏振是敏感的, 因此需要利用偏振控制器调控输入光束的偏振态, 以满足阵列波导光栅芯片的需求。然后调整偏振态的光束, 在红外成像系统的监视下, 利用位移台不断调节锥形光纤与阵列波导芯片的输入端的位置, 使输入光能够以最小的耦合损耗进入到芯片中。之后在芯片的输出端口放置 8 通道的阵列光纤, 每个光纤分别对应一个输出通道。最后用光谱仪依次记录每个通道的输出光谱, 即可得到阵列波导光栅芯片的输出结果。

对硅波导阵列波导光栅芯片进行测试, 其测试光谱如图 7 所示, 该芯片实现了 8 通道 200 GHz 的波分复用, 其结构尺寸仅为  $294 \mu\text{m} \times 190 \mu\text{m}$ 。根据相关定义计算出各性能参数, 插入损耗的最小值为 19.6 dB, 串扰为 -15 dB, 通道的非均匀性为 0.87 dB, 3 dB 带宽为 1.06 nm。测试的插入损耗主要来源于测试系统的耦合损耗和阵列波导光栅的片上损耗。其中耦合损耗大约为 10 dB, 阵列波导光栅的片上损耗为 9.6 dB。从结果可以看出, 该芯片的损耗还是非常大的, 因此需要针对各部分的损耗分别进行优化改进。针对耦合损耗,

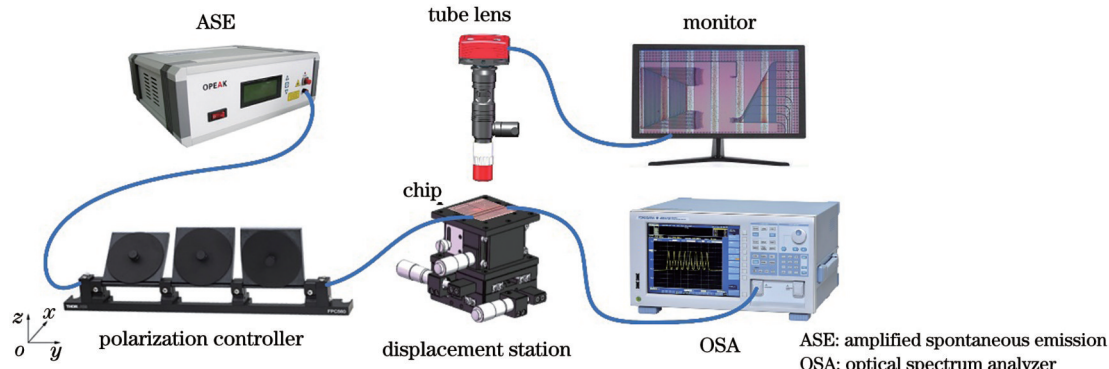


图 6 测试系统示意图

Fig. 6 Schematic of test system

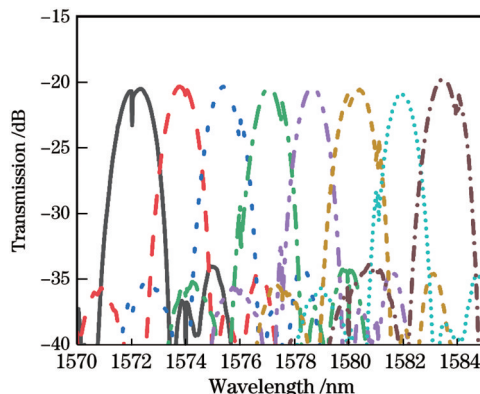


图 7 实验测得的 8 通道 200 GHz 硅波导阵列波导光栅的输出

光谱

Fig. 7 Output spectra of 8-channel 200 GHz silicon waveguide arrayed waveguide grating measured by experiment

目前端面耦合波导的宽度为 200 nm, 可通过采用更高精度的光刻技术将尺寸减小至约 120 nm, 以减小波导模式形貌与耦合光纤的模斑失配量。此外, 可对芯片进行封装, 减小测量的误差和损耗。针对阵列波导光栅的片上损耗, 可通过进一步优化设计光栅结构, 在保证器件尺寸和性能不被影响的情况下, 减小阵列波导之间的间距, 通过渐变结构进一步减小插入损耗。该器件采用与互补金属氧化物半导体工艺相兼容的绝缘体上硅技术, 因此能够实现大批量、低成本生产, 同时该器件具有结构紧凑、均匀性高的特点, 对高度集成的波分复用网络的发展具有重要的意义。

### 4 结 论

设计并制作了一种结构紧凑的高均匀性硅波导阵

列波导光栅芯片,该芯片含有 8 个输出通道并且通道间隔为 200 GHz,其尺寸仅为  $294 \mu\text{m} \times 190 \mu\text{m}$ 。为了减小器件尺寸,验证了波导弯曲半径对波导弯曲损耗和有效折射率的影响。对芯片进行测试,器件插入损耗的最小值为 19.6 dB,串扰为 -15 dB,通道的非均匀性为 0.87 dB,3 dB 带宽为 1.06 nm。该器件具有结构紧凑、均匀性高的特点,并且制作过程采用了与互补金属氧化物半导体工艺相兼容的绝缘体上硅技术,因此能够实现大批量、低成本生产,这有利于高度集成的波分复用网络的发展。

## 参考文献

- [1] 王亮亮, 张家顺, 安俊明, 等. 紧凑低损耗粗波分解复用芯片[J]. 光学学报, 2021, 41(9): 0923001.  
Wang L L, Zhang J S, An J M, et al. Compact and low loss coarse wavelength division demultiplexer chip[J]. Acta Optica Sinica, 2021, 41(9): 0923001.
- [2] Marom D M, Blau M. Switching solutions for WDM-SDM optical networks[J]. IEEE Communications Magazine, 2015, 53(2): 60-68.
- [3] Ismail N, Sun F, Sengo G, et al. Improved arrayed-waveguide-grating layout avoiding systematic phase errors[J]. Optics Express, 2011, 19(9): 8781-8794.
- [4] Obaid H M, Shahid H. Performance evaluation of hybrid optical amplifiers for a  $100 \times 10$  Gbps DWDM system with ultrasmall channel spacing[J]. Optik, 2020, 200: 163404.
- [5] Blau M, Marom D M. Spatial aperture-sampled mode multiplexer extended to higher mode count fibers[J]. Journal of Lightwave Technology, 2015, 33(23): 4805-4814.
- [6] Chen Y H, Tang W J. Reconfigurable asymmetric optical burst switching for concurrent DWDM multimode switching: architecture and research directions[J]. IEEE Communications Magazine, 2010, 48(5): 57-65.
- [7] Stanton E J, Spott A, Davenport M L, et al. Low-loss arrayed waveguide grating at 760 nm[J]. Optics Letters, 2016, 41(8): 1785-1788.
- [8] Fotiadis K, Pitriss S, Moralidis-Pegios M, et al. Silicon photonic  $16 \times 16$  cyclic AWGR for DWDM O-band interconnects[J]. IEEE Photonics Technology Letters, 2020, 32(19): 1233-1236.
- [9] 原荣. 阵列波导光栅(AWG)器件及其应用[J]. 光通信技术, 2010, 34(1): 1-5.  
Yuan R. Arrayed waveguide grating component and its applications [J]. Optical Communication Technology, 2010, 34(1): 1-5.
- [10] Kamei S, Ishii M, Itoh M, et al. 64  $\times$  64-channel uniform-loss and cyclic-frequency arrayed-waveguide grating router module[J]. Electronics Letters, 2003, 39(1): 83.
- [11] 张家顺, 安俊明, 孙冰丽, 等. 硅基二氧化硅 20 通道循环型阵列波导光栅制备[J]. 光子学报, 2022, 51(6): 0623003.  
Zhang J S, An J M, Sun B L, et al. Fabrication of silica based silicon 20 channel cyclic arrayed waveguide grating[J]. Acta Photonica Sinica, 2022, 51(6): 0623003.
- [12] 冉娜, 陈昕阳, 汪正坤, 等. 氮化硅片上光栅耦合器的优化和实验[J]. 光学学报, 2023, 43(1): 0113002.  
Ran N, Chen X Y, Wang Z K, et al. Optimization and experiments of on-chip silicon nitride grating couplers[J]. Acta Optica Sinica, 2023, 43(1): 0113002.
- [13] Smit M K. New focusing and dispersive planar component based on an optical phased array[J]. Electronics Letters, 1988, 24(7): 385.
- [14] Doerr C R, Zhang L M, Winzer P J. Monolithic InP multiwavelength coherent receiver using a chirped arrayed waveguide grating[J]. Journal of Lightwave Technology, 2011, 29(4): 536-541.
- [15] Takada K, Yamada H, Inoue Y. Optical low coherence method for characterizing silica-based arrayed-waveguide grating multiplexers[J]. Journal of Lightwave Technology, 1996, 14(7): 1677-1689.
- [16] Lu S, Yang C X, Yan Y B, et al. Design and fabrication of a polymeric flat focal field arrayed waveguide grating[J]. Optics Express, 2005, 13(25): 9982-9994.
- [17] Li C Y, An J M, Wang J Q, et al. The  $8 \times 10$  GHz receiver optical subassembly based on silica hybrid integration technology for data center interconnection[J]. Chinese Physics Letters, 2017, 34(10): 104202.
- [18] Min Y H, Lee M H, Ju J J, et al. Polymeric  $16 \times 16$  arrayed-waveguide grating router using fluorinated polyethers operating around 1550 nm[J]. IEEE Journal of Selected Topics in Quantum Electronics, 2001, 7(5): 806-811.
- [19] Wang J, Sheng Z, Li L, et al. Low-loss and low-crosstalk  $8 \times 8$  silicon nanowire AWG routers fabricated with CMOS technology [J]. Optics Express, 2014, 22(8): 9395-9403.
- [20] Park J, Joo J, Kwack M J, et al. Three-dimensional wavelength-division multiplexing interconnects based on a low-loss  $\text{Si}_x\text{N}_y$  arrayed waveguide grating[J]. Optics Express, 2021, 29(22): 35261-35270.
- [21] Zou J, Jiang X X, Xia X, et al. Ultra-compact birefringence-compensated arrayed waveguide grating triplexer based on silicon-on-insulator[J]. Journal of Lightwave Technology, 2013, 31(12): 1935-1940.
- [22] 刘大建, 赵伟科, 张龙, 等. 高性能无源硅光波导器件: 发展与挑战[J]. 光学学报, 2022, 42(17): 1713001.  
Liu D J, Zhao W K, Zhang L, et al. High performance passive silicon optical waveguide devices: development and challenges[J]. Acta Optica Sinica, 2022, 42(17): 1713001.
- [23] 孙道鑫, 张东亮, 毕付, 等. 应用于集成光学陀螺敏感单元的硅基微环谐振腔[J]. 激光与光电子学进展, 2022, 59(13): 1313001.  
Sun D X, Zhang D L, Bi F, et al. Application of silicon-based microring resonant cavity in integrated optical gyroscope sensitive unit[J]. Laser & Optoelectronics Progress, 2022, 59(13): 1313001.
- [24] Liu H P, Feng J J, Ge J M, et al. Tilted nano-grating based ultra-compact broadband polarizing beam splitter for silicon photonics[J]. Nanomaterials, 2021, 11(10): 2645.
- [25] Nishi H, Tsuchizawa T, Kou R, et al. Monolithic integration of a silica AWG and Ge photodiodes on Si photonic platform for one-chip WDM receiver[J]. Optics Express, 2012, 20(8): 9312-9321.
- [26] Yuan S, Feng J J, Yu Z H, et al. Silicon nanowire-assisted high uniform arrayed waveguide grating[J]. Nanomaterials, 2022, 13(1): 182.
- [27] Pathak S, Vanslembrouck M, Dumon P, et al. Optimized silicon AWG with flattened spectral response using an MMI aperture[J]. Journal of Lightwave Technology, 2013, 31(1): 87-93.
- [28] Li H Q, Gao W T, Li E B, et al. Investigation of ultrasmall  $1 \times N$  AWG for SOI-based AWG demodulation integration microsystem [J]. IEEE Photonics Journal, 2015, 7(6): 7802707.
- [29] Marz R, Cremer C. On the theory of planar spectrographs[J]. Journal of Lightwave Technology, 1992, 10(12): 2017-2022.
- [30] Smit M K, Van Dam C. PHASAR-based WDM-devices: principles, design and applications[J]. IEEE Journal of Selected Topics in Quantum Electronics, 1996, 2(2): 236-250.
- [31] Zou J, Ma X, Xia X, et al. High resolution and ultra-compact on-chip spectrometer using bidirectional edge-input arrayed waveguide grating[J]. Journal of Lightwave Technology, 2020, 38(16): 4447-4453.
- [32] Song G Y, Wang S X, Zou J, et al. Silicon-based cyclic arrayed waveguide grating routers with improved loss uniformity[J]. Optics Communications, 2018, 427: 628-634.
- [33] Lu H C, Wang W S. Cyclic arrayed waveguide grating devices with flat-top passband and uniform spectral response[J]. IEEE Photonics Technology Letters, 2008, 20(1): 3-5.
- [34] 刘晓腾, 冯吉军, 吴昕耀, 等. 基于硅基波导的集成光学相控阵

芯片(特邀)[J]. 光子学报, 2020, 49(11): 1149012.

Liu X T, Feng J J, Wu X Y, et al. Silicon waveguide based

integrated optical phased array chips (invited)[J]. Acta Photonica Sinica, 2020, 49(11): 1149012.

## Compact High Uniformity Silicon Waveguide Arrayed Waveguide Grating

Feng Zhihua<sup>1,4</sup>, Yuan Shuo<sup>2</sup>, Chen Yishu<sup>2</sup>, Liu Haipeng<sup>2</sup>, Bi Qunyu<sup>3</sup>, Zhang Fuling<sup>4\*</sup>,  
Feng Jijun<sup>2\*\*</sup>

<sup>1</sup>School of Physics, Xidian University, Xi'an 710071, Shaanxi, China;

<sup>2</sup>Shanghai Key Laboratory of Modern Optical System, University of Shanghai for Science and Technology,  
Shanghai 200093, China;

<sup>3</sup>Key Lab of Advanced Optical Manufacturing Technologies of Jiangsu Province, Soochow University, Suzhou 215006,  
Jiangsu, China;

<sup>4</sup>The 27th Research Institute, China Electronics Technology Group Corporation, Zhengzhou 450047, Henan, China

### Abstract

**Objective** With the rapid development of large traffic network, the demand for data exchange rates is increasing daily. Wavelength-division multiplexing (WDM) has garnered considerable attention in optical communication networks owing to its high communication speed, transparent signal transmission, efficient expansion of transmission capacity, and low cost. Dense wavelength division multiplexing (DWDM) is a crucial component of the optical communication field because it increases the capacity of communication systems and satisfies the public demand for greater communication bandwidth. Arrayed waveguide gratings (AWG) have low crosstalk, low insertion loss, high uniformity, high reliability, and a compact structure. Therefore, they have become the most commonly employed technical solution for DWDM. AWGs have been demonstrated in low-refractive-index-contrast materials, such as InP, silica, and polymers. The refractive-index contrast of the core and cladding of these materials is low; therefore, the device size and bending loss are large, which is unfavorable for the development of highly integrated DWDM systems. Owing to the high refractive-index contrast, a silicon waveguide arrayed waveguide grating can be made extremely compact, allowing for low-cost and high-volume manufacturing owing to its complementary metal-oxide semiconductor (CMOS)-compatible processing. Many arrayed waveguide gratings using silicon waveguides have been proposed. However, they still need to be further reduced in size to increase integration, and the uniformity of each output channel needs to be improved.

**Methods** A compact, highly uniform silicon-arrayed waveguide grating is studied. First, the arrayed waveguide grating is theoretically analyzed to understand its design scheme and performance parameters. Subsequently, the waveguide bending loss and effective index versus the silicon waveguide bending radius are simulated (Fig. 3). With a gradual decrease in the bending radius, the bending loss and effective index first decrease and then stabilize. When the bending radius is between 2.5 μm and 5.0 μm, the bending loss exceeds 1.29 dB, and the effective index of the silicon waveguide is greatly affected by the bending radius. When the bending radius exceeds 15 μm, the bending loss is less than 0.028 dB. The silicon waveguide's bending loss is negligible, and the effective index of the waveguide is stable at 2.449. According to the comprehensive consideration of device performance, the bending radius is 15 μm. Finally, according to the basic principles of arrayed waveguide gratings and the related parameters of silicon waveguides, the main structural parameters of the compact and highly uniform silicon waveguide arrayed waveguide gratings are determined (Table 1). Subsequently, a compact silicon-arrayed waveguide grating is fabricated on a silicon on insulator (SOI) platform. Finally, a test system is built to obtain the spectral characteristics of the silicon-arrayed waveguide grating chip, and each parameter is presented.

**Results and Discussions** In this study, a silicon-arrayed waveguide grating chip is prepared and tested. The chip realizes 8-channel 200-GHz WDM, and its structure size is only 294 μm × 190 μm. The performance of each parameter is calculated according to the relevant definitions. The minimum insertion loss value is 19.6 dB, crosstalk is -15 dB, nonuniformity of the channel is 0.87 dB, and 3 dB bandwidth is 1.06 nm. The insertion loss during the testing process mainly originates from the coupling loss of the test system and the on-chip loss of the arrayed waveguide grating. The coupling loss is approximately 10 dB, and the on-chip loss of the arrayed waveguide grating is 9.6 dB. The device adopts silicon-on-insulator technology compatible with the CMOS process; therefore, its mass and low-cost production can be realized. In addition, the device has a compact structure and high uniformity.

**Conclusions** Based on a silicon-on-insulator material platform, a compact highly uniform silicon waveguide-arrayed grating with eight output channels and a channel spacing of 200 GHz is designed and fabricated. The effects of the bending radius of the silicon waveguide on the bending loss and effective refractive index of the silicon-on-insulator platform are analyzed. The test results show that the insertion loss of the device is 19.6 dB, the crosstalk is -15 dB, the nonuniformity is 0.87 dB, the 3 dB bandwidth is 1.06 nm, and the structure size is only 294 μm × 190 μm. The chip can be produced using a CMOS process, which enables the production of arrayed waveguide gratings in large quantities at low cost. This is crucial for the development of integrated WDM networks.

**Key words** integrated optics; arrayed waveguide grating; compact structure; silicon waveguide; wavelength division multiplexing